Head-to-Head Comparison of ^{68}Ga-PSMA-11 with ^{18}F-PSMA-1007 PET/CT in Staging Prostate Cancer Using Histopathology and Immunohistochemical Analysis as a Reference Standard

Jonathan Kuten[1], Ibrahim Fahoum[2], Ziv Savin[3], Ofer Shamni[4], Gilad Gitstein[2], Dov Hershkovitz[2,5], Nicola J. Mabjeesh[3,5], Ofer Yossepowitch[3,5], Eyal Mishani[4], and Einat Even-Sapir[1,5]

[1]Department of Nuclear Medicine, Tel Aviv Sourasky Medical Center, Tel Aviv, Israel; [2]Department of Pathology, Tel Aviv Sourasky Medical Center, Tel Aviv, Israel; [3]Department of Urology, Tel Aviv Sourasky Medical Center, Tel Aviv, Israel; [4]Hadassah Cyclotron Unit, Hadassah Medical Center, Jerusalem, Israel; and [5]Sackler Faculty of Medicine, Tel Aviv University, Tel Aviv, Israel

^{18}F-PSMA-1007 is a novel prostate-specific membrane antigen (PSMA)–based radiopharmaceutical for imaging prostate cancer (PCa). The aim of this study was to compare the diagnostic accuracy of ^{18}F-PSMA-1007 with ^{68}Ga-PSMA-11 PET/CT in the same patients presenting with newly diagnosed intermediate- or high-risk PCa. **Methods:** Sixteen patients with intermediate- or high-risk PCa underwent ^{18}F-PSMA-1007 and ^{68}Ga-PSMA-11 PET/CT within 15 d. PET findings were compared between the 2 radiotracers and with reference-standard pathologic specimens obtained from radical prostatectomy. The Cohen κ-coefficient was used to assess the concordance between ^{18}F-PSMA-1007 and ^{68}Ga-PSMA-11 for detection of intraprostatic lesions. The McNemar test was used to assess agreement between intraprostatic PET/CT findings and histopathologic findings. Sensitivity, specificity, positive predictive value, and negative predictive value were reported for each radiotracer. SUV_{max} was measured for all lesions, and tumor-to-background activity was calculated. Areas under receiver-operating-characteristic curves were calculated for discriminating diseased from nondiseased prostate segments, and optimal SUV cutoffs were calculated using the Youden index for each radiotracer. **Results:** PSMA-avid lesions in the prostate were identified in all 16 patients with an almost perfect concordance between the 2 tracers (κ ranged from 0.871 to 1). Aside from the dominant intraprostatic lesion, similarly detected by both radiotracers, a second less intense positive focus was detected in 4 patients only with ^{18}F-PSMA-1007. Three of these secondary foci were confirmed as Gleason grade 3 lesions, whereas the fourth was shown on pathologic examination to represent chronic prostatitis. **Conclusion:** This pilot study showed that both ^{18}F-PSMA-1007 and ^{68}Ga-PSMA-11 identify all dominant prostatic lesions in patients with intermediate- or high-risk PCa at staging. ^{18}F-PSMA-1007, however, may detect additional low-grade lesions of limited clinical relevance.

Key Words: ^{18}F-PSMA-1007; ^{68}Ga-PSMA-11; prostate cancer; comparison; staging

J Nucl Med 2020; 61:527–532
DOI: 10.2967/jnumed.119.234187

Received Jul. 18, 2019; revision accepted Aug. 26, 2019.
For correspondence or reprints contact: Einat Even-Sapir, Tel Aviv Sourasky Medical Center, 6 Weizmann St., Tel-Aviv, 6423906, Israel.
E-mail: evensap@tlvmc.gov.il
Published online Sep. 27, 2019.

Prostate-specific membrane antigen (PSMA) is a transmembrane glycoprotein overexpressed in prostate cancer (PCa) cells. Several radiolabeled PSMA probes have been developed, including that most widely used: ^{68}Ga-PSMA-11. It is well established that ^{68}Ga-PSMA-11 PET/CT is superior to conventional imaging and to choline-based PET/CT for evaluating PCa patients, primarily in the context of biochemical failure but also for staging purposes (*1–13*). ^{18}F-PSMA-1007 is a novel PSMA-based radiopharmaceutical that has several advantages over ^{68}Ga-PSMA-11. ^{18}F-labeled agents enable large-scale radiosynthesis, allowing for a larger number of patient studies, as compared with the limited quantity obtained from the generator-produced ^{68}Ga. In addition, the longer physical half-life of the ^{18}F radioisotope (half-life, 109 min) allows for central production and distribution to satellite centers. ^{18}F-PSMA-1007 may also offer images of higher spatial resolution than are possible with ^{68}Ga because of the relatively low positron energy of ^{18}F (average β^+ energy, 250 keV) (*14,15*).

Another clear advantage of ^{18}F-PSMA-1007 over ^{68}Ga-PSMA-11, ^{68}Ga-PSMA-617, and the available fluorinated PSMA derivative, ^{18}F-DCFPyL, is the lack of renal excretion and the low urinary activity, which can benefit clinical decision making in cases of local recurrence and unclear lesions near the ureter or urinary bladder (*16*). ^{18}F-PSMA-1007 has a structural scaffold similar to that of ^{68}Ga-PSMA-617, resulting in similar distribution kinetics. This similarity makes ^{18}F-PSMA-1007 optimal for stratifying patients according to their suitability for therapy with ^{177}Lu-PSMA-617 (*17*). Recently, ^{18}F-PSMA-1007 was shown to have detection rates comparable to or higher than ^{68}Ga-labeled PSMA ligands in biochemical failure (*18,19*).

The aim of this study was to compare the findings of ^{18}F-PSMA-1007 PET/CT and ^{68}Ga-PSMA-11 PET/CT in the same patients presenting with newly diagnosed intermediate- or high-risk PCa using histopathology and immunohistochemical staining as reference standards.

MATERIALS AND METHODS

This was a prospective study. ^{18}F-PSMA-1007 and ^{68}Ga-PSMA-11 PET/CT were performed within 15 d of each other (median interval, 6 d) in 16 patients with intermediate-risk PCa (prostate-specific antigen [PSA] of 10–20 ng/mL or Gleason score ≥ 7 or ≥ cT2b) or high-risk PCa (PSA > 20 ng/mL or GS ≥ 8 or cT3) (*20*) scheduled to undergo radical prostatectomy. The study was approved by the institutional ethical committee (reference number, 0765-17-TLV). This study was

also registered with the Israeli Ministry of Health (reference number, MOH_2018-01-11_002026) and with the National Institutes of Health (reference number TASMC-17-ES-0765-CTIL). The study protocol is available as supplemental data (supplemental materials are available at http://jnm.snmjournals.org). All patients gave written informed consent to have 2 consecutive labeled PSMA PET/CT studies.

Findings with the 2 PET tracers were compared with histopathologic findings obtained from radical prostatectomy specimens, considered the reference standard.

Intraprostatic pathologic lesions on PET/CT were drawn on a customized scheme of the prostate (Supplemental Fig. 1) divided into upper, middle, and lower thirds; left or right lobes; central or peripheral regions; and anterior or posterior regions. The same scheme of the prostate gland was used by the uropathologist to specify the location of malignant lesions found on prostatectomy specimens. The nuclear medicine physicians and uropathologists were masked to one another's results. For the purpose of analysis, the prostate was divided into 6 distinct segments, namely base right/left, mid right/left, and apex right/left.

^{18}F-PSMA-1007 and ^{68}Ga-HBED-CC Synthesis

^{68}Ga-PSMA-11. The ^{68}Ga-PSMA-11 was synthesized using an Isotope Technologies Garching GmBH ^{68}Ge/^{68}Ga generator and a semiautomated module in a good-manufacturing-practice–compliant process (*21*). The radiolabeling was performed over 5 min using a disposable cassette, labeling kit, and 10 μg of PSMA-HBED-CC (ABX GmBH) precursor dissolved in 1 mL of sodium acetate buffer (0.25 M). The final product identity and purity were confirmed using analytic high-performance liquid chromatography, and radiochemical purity was routinely over 99%. The final product was subjected to quality control analyses in compliance with the European Pharmacopoeia.

^{18}F-PSMA-1007. The ^{18}F-PSMA-1007 was synthesized by a fully automated process as was previously described (*22*). In brief, after trapping the (^{18}F)/$H_2{}^{18}O$ from the target, it was loaded onto an anion exchange column (30PS-HCO3; Macherey Nagel), eluted using 0.65 mL of thiobarbituric acid solution (0.075 M; ABX GmBH), and transferred to the reactor followed by addition of 1.5 mL of acetonitrile (Across Organics) and azeotropic removal of water. PSMA-1007 precursor (1 mg) dissolved in 1 mL of anhydrous dimethyl sulfoxide was then added, and radiolabeling was performed at 90°C for 3 min. The reaction crud was then diluted with 15 mL of 10% ethanol and loaded onto consecutive solid-phase extraction cartridges (PSH+ and C18ec; Macherey Nagel) followed by an additional 10 mL of 15% ethanol. The final product was eluted using 3.5 mL of 40% ethanol, diluted with 16.5 mL of 0.9% NaCl solution, supplemented with 100 mg of sodium ascorbate, and filter-sterilized using a 0.22-μm filter (Cathivex-GV). Identification of the ^{18}F-PSMA-1007 was confirmed by coelution with the reference standard using analytic high-performance liquid chromatography, and the radiochemical purity was 96.3% ± 0.5% (n = 24). The final product quality control was in compliance with previously described acceptance criteria (*23*).

Imaging Procedure

PET/CT studies were performed on separate days using the Discovery 690 PET/CT system (GE Healthcare). All patients were examined on the same scanner. Patients were instructed to drink 500 mL of water during a 2-h period before acquisition and to void immediately before the start of acquisition. Imaging was done from the tip of the skull to the mid thigh. ^{68}Ga-PSMA-11 was injected 45–80 min before acquisition started (*24*), and ^{18}F-PSMA-1007 was injected as a bolus 60 min before acquisition.

The CT acquisition was performed using automatic current modulation and 120 kV, and the images were reconstructed to a slice thickness of 2.5 mm. The PET acquisition was performed at 3 min per bed position in 3-dimensional mode, and the images were reconstructed in a 128 × 128 matrix with a pixel size of 5.5 mm and a slice thickness of 3.3 mm. The reconstruction method was VUE Point FX (GE Healthcare), which uses time-of-flight information and includes a fully 3-dimensional ordered-subsets expectation maximization algorithm with 2 iterations, 24 subsets, and a filter cutoff of 6.4 mm. The VUE Point FX algorithm also includes normalization and image corrections for attenuation, scatter, randoms, and dead time. A standard Z-filter was applied to smooth between transaxial slices. The same reconstruction parameters were used for both radiotracers.

Image Analysis

All scans were reviewed by nuclear medicine physicians experienced in interpretation of labeled PSMA PET studies, on a computer-assisted reading application (AW Server, version 3.2; GE Healthcare), which allowed the review of PET, CT, and fused imaging data in axial, coronal, and sagittal slices. Intraprostatic lesions were judged as positive when radiotracer uptake was focal and higher than that of surrounding prostate tissue, as previously described (*25,26*). Outside the prostate, a pathologic lesion was considered as any soft-tissue or skeletal lesion showing increased uptake above normal surroundings (*8,27*). Typical pitfalls in PSMA ligand PET imaging were considered (*25,28*). For calculation of the SUV_{max} of the primary tumor, volumes of interest were segmented automatically with a manually adapted isocontour threshold centered on lesions with focally increased uptake, as previously described (*25*).

SUV_{max} in each segment of the prostate was measured using a 1-cm spheric volume of interest.

Tumor-to-background SUV_{max} ratio was calculated for each lesion. For background activity, 2-dimensional 2 ± 0.03 cm^2 (median ± SD) ROIs were semiautomatically drawn on the normal prostate, left gluteal maximus muscle, and mediastinal blood pool. These areas were chosen as background in accordance with previous studies (*13,25*). SUV_{max} was chosen because it is considered more operator-independent and more suitable for smaller lesions (*1*). SUV_{mean} in the urinary bladder was automatically calculated from volumes of interest that were segmented automatically with a manually adapted isocontour threshold based on physiologic urine uptake and verified using anatomic CT data. SUV_{mean} was chosen because it is more suitable for measuring uptake in a large homogeneous structure such as the bladder.

Surgery

Fifteen patients underwent robot-assisted laparoscopic radical prostatectomy with pelvic lymph node dissection, including removal of lymphatic packages along the internal and external iliac vessels and obturator fossa. One patient had unanticipated evidence of gross metastatic lesions observed during his preoperative workup, and he declined his surgery.

Histopathology and Immunostaining

Radical prostatectomy specimens were embedded in formalin, and the right and left halves of the gland were inked in 2 different colors to maintain its orientation. After sampling the proximal margin (prostate base), the distal apical margin, and the base of each seminal vesicle separately, we sectioned the remaining prostate serially at 5-mm slices from base to apex perpendicular to the urethral axis. The slices were laid out sequentially and divided into an upper third (slices adjacent to the base), a middle third, and a lower third (slices adjacent to the apex). After overnight fixation, representative sections were taken from all thirds. In the absence of whole-mount processing, each slice was further divided into 4 quadrants (right anterior, left anterior, right posterior, and left posterior). Each quadrant was placed in a cassette labeled with its location (e.g., cassette no. 5—upper third, right posterior). Hematoxylin- and eosin-stained slides were prepared from all samples using standard methods. Histologic evaluation and Gleason grading were performed by a dedicated genitourinary pathologist in accordance with criteria established by the International Society of Uropathologists. Tumor areas were mapped according to the location of the samples containing prostatic malignant tissue.

PSMA immunohistochemical staining was performed on selected samples using monoclonal anti-PSMA antibody (clone 3E6, dilution

TABLE 1
Characteristics of Patients

Patient no.	Clinical stage	Age (y)	GS	PSA (ng/mL)	Clinical risk class	Dominant-lesion location	Dominant-lesion grade group	^{18}F SUV_{max}	^{68}Ga SUV_{max}	Second-lesion ^{18}F	Second-lesion ^{68}Ga	^{18}F second-lesion SUV_{max}	^{68}Ga second-lesion SUV_{max}	Second-lesion pathologic evaluation
1	T1c	71	4 + 3	7.7	Unfavorable intermediate	Left base–mid apex	4	57.15	36.79					
2	T1c	74	3 + 3	10.7	Favorable intermediate	Right base–mid apex	2	6.32	3.38	Left apex		3.62		True-positive (Gleason pattern 3)
3	T2a	69	4 + 3	6.8	Unfavorable intermediate	Right mid gland and apex	2	5.49	4.72					
4	T1c	67	4 + 4	4.9	High	Left mid gland and apex	3	23.55	9.50	Right apex		5.55		True-positive (Gleason pattern 3)
5	T1c	69	4 + 4	5.49	High	Left mid gland and apex	2	8.06	3.30	Right mid gland	Right mid gland	6.43	3.28	Faslse-positive (chronic prostatitis)
6	T1c	72	4 + 3	5	Unfavorable intermediate	Left base–mid apex	3	11.42	7.90					
7	T1c	71	4 + 3	13.2	Unfavorable intermediate	Left base–mid apex	2	13.63	9.86					
8	T1c	60	3 + 4	5.9	Favorable intermediate	Left base	2	4.59	2.74					
9	T1c	62	4 + 3	19	Unfavorable intermediate	Not applicable	Not applicable	8.19	12.30					
10	T2c	71	3 + 4	5.7	High	Right base and mid gland	3	6.93	6.40					
11	T1c	68	3 + 4	3.5	Favorable intermediate	Left base and mid gland	2	8.64	7.48					
12	T1c	66	4 + 4	4.9	High	Right base–mid apex	3	11.45	6.19	Left mid gland		4.20		False-positive (chronic prostatitis)
13	T1c	65	3 + 3	14.44	Favorable intermediate	Left and right apex	2	17.15	11.40					
14	T1c	59	3 + 4	9.6	Favorable intermediate	Right base–mid apex	3	6.80	5.04					
15	T1c	72	4 + 3	5.4	Unfavorable intermediate	Right mid gland and apex	3	15.03	9.16					
16	T1c	56	3 + 4	11	Unfavorable intermediate	Right mid gland and apex	2	8.83	2.29	Left apex		3.34		True-positive (Gleason pattern 3)

GS = Gleason score.

1/100; Dako). The stained samples were evaluated by 2 pathologists according to the percentage of positively stained cells and the staining intensity (0, no color; +1, weak; +2, moderate; +3, intense).

Statistical Analysis

For statistical analysis, 6 major segments of the prostate were used (base right/left, mid right/left, and apex right/left). Categoric variables were reported as frequency and percentage, and continuous variables were reported as median and interquartile range. The Cohen κ-coefficient was used to assess the concordance between ^{18}F-PSMA-1007 and ^{68}Ga-PSMA-11 for detection of intraprostatic lesions. Interpretation of κ-values was according to Landis and Koch (*29*). The Wilcoxon test was used to compare SUV_{max} between ^{18}F-PSMA-1007 and ^{68}Ga-PSMA-11 in the prostate lesions and in the bladder.

The Spearman correlation coefficient was used to assess correlation between SUV_{max} difference and the following patient characteristics: age, body mass index, Gleason score, PSA, and clinical stage. The McNemar test was used to assess agreement between intraprostatic PET/CT findings and histopathologic findings. The areas under receiver-operating-characteristic curves were calculated for each prostate segment and for all segments pooled together in order to describe the overall and per-segment discriminatory ability between diseased and nondiseased areas for each radiotracer.

The Youden index was used to calculate the optimal SUV cutoff for detecting dominant lesions for each segment and for all segments pooled together. On the basis of these cutoffs, we reported sensitivity, specificity, positive predictive value, negative predictive value, and accuracy for each radiotracer for the 15 patients with a histopathologic reference standard. All statistical tests were 2-sided, and a P value of less than 0.05 was considered statistically significant. SPSS was used for all statistical analyses (version 25.0; IBM Corp., for Windows [Microsoft]).

RESULTS

The patients' characteristics are summarized in Table 1 and Supplemental Table 1. Patients were categorized into risk groups as previously described (*30,31*). Labeled PSMA-avid lesions in the prostate were identified in all 16 patients, with almost perfect agreement between the 2 tracers (Supplemental Table 2) regarding tumor location ($\kappa = 0.871–1$).

Median SUV_{max} in the primary dominant intraprostatic tumors was higher for ^{18}F-PSMA-1007 than for ^{68}Ga-PSMA-11, at 8.73 and 6.94, respectively ($P = 0.002$). The difference in SUV_{max} between the 2 tracers, both in prostatic lesions and outside the prostate, was not associated with patient age, body mass index, Gleason score, PSA, or clinical stage (Spearman correlation coefficient was used for this analysis). Normal background median SUV_{max} was also higher for ^{18}F-PSMA-1007 than for ^{68}Ga-PSMA-11 in all regions of interest measured, including normal prostate (2.57 and 1.85, respectively; $P = 0.001$), left gluteus maximus muscle (0.675 and 0.53, respectively; $P = 0.001$), and mediastinal blood pool (1.96 and 0.975, respectively; $P = 0.001$). No significant difference was found in any lesion-to-background SUV_{max} ratio between the 2 tracers. Urinary excretion was significantly lower for ^{18}F-PSMA-1007 than for ^{68}Ga-PSMA-11. Median urinary bladder SUV_{mean} was 3.66 and 25.35, respectively ($P < 0.001$). Ureteric activity was viewed in all ^{68}Ga-PSMA-11 scans, as opposed to only one ^{18}F-PSMA-1007 PET/CT scan (Fig. 1; Supplemental Figs. 2–17).

Aside from the dominant intraprostatic lesion, which was detected by both radiotracers, in 4 patients a second positive focus, though less intense, was detected only by ^{18}F-PSMA-1007 PET/CT. Three of these secondary lesions were confirmed as true-positive sites of prostatic adenocarcinoma with Gleason grade 3 and moderate PSMA staining on pathologic specimens. The fourth lesion evident only on ^{18}F-PSMA-1007 PET/CT was shown on pathologic examination to be a false-positive focus of chronic prostatitis associated with weak positive staining for PSMA.

Median SUV_{max} was significantly higher in the primary dominant lesion than in secondary lesions detected by ^{18}F-PSMA-1007 (8.73 and 4.2, respectively; $P = 0.043$). Intraprostatic findings on PET/CT and histopathology are summarized in Supplemental Table 3. Both radiotracers were able to discriminate well between dominant lesions and nondiseased segments of the prostate (Supplemental Table 4). Sensitivity, specificity, positive predictive value, negative predictive value, and accuracy for detecting dominant lesions were 100, 90.9, 87.5, 100, and 94.5, respectively, for ^{18}F-PSMA-1007 and 85.7, 98.2, 96.8, 91.5, and 93.3, respectively, for ^{68}Ga-PSMA-11 (Supplemental Table 5). Regarding nondominant lesions, the areas under the curve per segment and for all segments pooled together did not significantly differ from 0.5; therefore, optimal SUV cutoffs were not calculated.

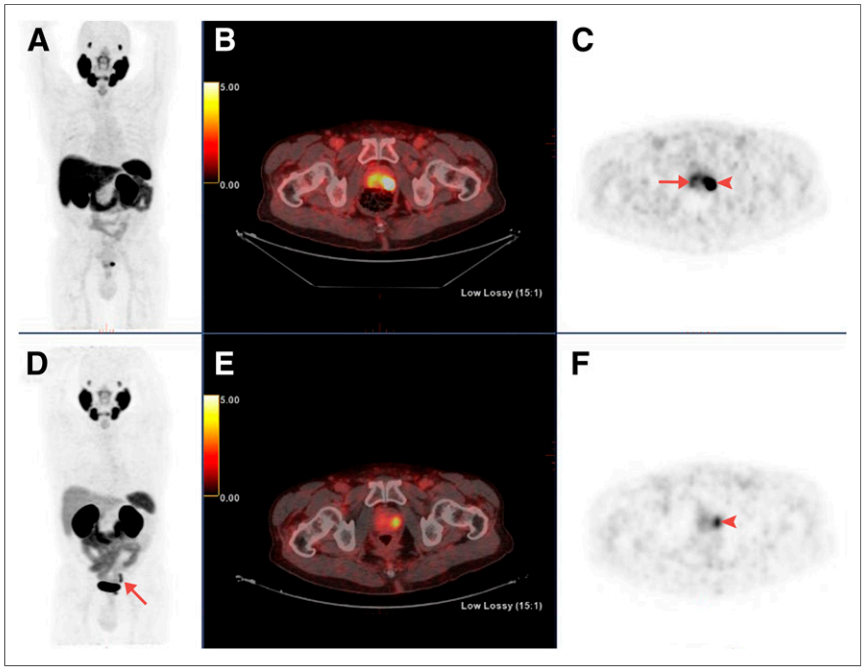

FIGURE 1. Maximum-intensity projections, transaxial fusion, and PET images of ^{18}F-PSMA-1007 (A–C) and ^{68}Ga-PSMA-11 (D–F) PET/CT scans of 67-y-old patient with GS 8 and PSA 4.9 ng/mL. Marked uptake is seen in urinary bladder and left ureter (arrow) on maximum-intensity projection image of ^{68}Ga-PSMA-11 (D), as opposed to nearly negligible ^{18}F-PSMA-1007 urinary excretion (A). Dominant lesion in left prostatic lobe is evident on both scans (arrowheads). However, second lesion is seen in right lobe only on ^{18}F-PSMA-1007 scan (arrow in C), later verified on pathology as true malignant lesion.

PSMA Immunohistochemical Staining

PSMA immunohistochemical staining of areas with chronic prostatitis and no evidence

of carcinoma was weak (+1) in approximately 30% of the cells (Fig. 2A). Compared with these areas, segments with prostatic adenocarcinoma showed stronger staining in a greater percentage of cells. The adenocarcinoma with the higher Gleason grade had more intense staining. The tumor area with Gleason grade 3 showed moderate staining (+2) in 80% of the tumor cells (Fig. 2B), and the adenocarcinoma with Gleason grade 4 had intense staining (+3) in over 90% of the tumor cells (Fig. 2C).

Extraprostatic Disease

No lymph node involvement was suggested in any of patients' PET/CT scans. Mild uptake was evident in one pelvic lymph node with both tracers and was interpreted as nonspecific. Pathologic examination of this lymph node showed calcification, but no explanation was found for the mild uptake. Overall, 145 lymph nodes were removed and available for pathologic evaluation; all were negative for carcinoma.

Other Findings

One patient had pathologic uptake in a blastic lesion in a thoracic vertebra, detected by both radiotracers and considered to be bone metastasis. Surgery was declined, and the patient was referred for radiation and hormonal therapy. One patient had mild uptake with both tracers (SUV_{max} of 3.35 and 1.7 for ^{18}F-PSMA-1007 and ^{68}Ga-PSMA-11, respectively) in a sclerotic lesion in a rib compatible with a healing fracture. This patient had undetectable levels of serum PSA at follow-up 8 mo after surgery.

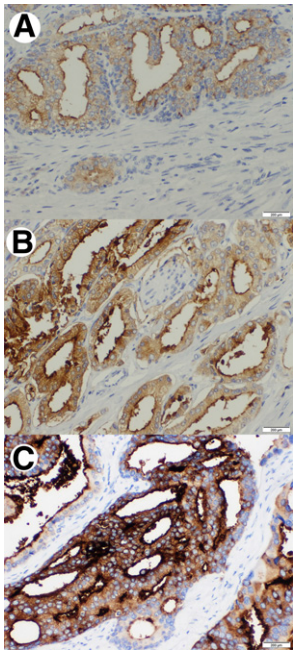

FIGURE 2. PSMA immunohistochemical stains in 3 different segments. (A) Area with chronic prostatitis showing weak staining (+1) in less than half of cells. (B) Area of prostatic adenocarcinoma, Gleason grade 3, with moderate staining (+2) of most tumor cells. (C) Area of prostatic adenocarcinoma, Gleason grade 4, showing intense staining (+3) in over 90% of tumor cells.

Follow-up

Clinical follow-up was available for 13 patients, with a median postsurgical interval of 173 d. All patients had undetectable levels of serum PSA except for one patient with positive surgical margins, found to have rising PSA levels 2 mo after surgery (from a 0.05 nadir to 0.2). This patient was referred for early salvage radiation therapy.

DISCUSSION

Imaging of PCa is an ongoing challenge, especially in the setting of staging intermediate- and high-risk patients. Previous reports have shown the usefulness of ^{68}Ga-PSMA-11 PET/CT for imaging PCa, as well as its superiority over morphologic imaging in the preoperative setting (*1–6*). Others have shown ^{68}Ga-PSMA-11 PET/CT to be superior to several other available radiotracers such as choline-based tracers (*7,9*) and ^{18}F-fluciclovine (*32*) in patients with recurrent PCa.

^{18}F-PSMA-1007 is a novel radiotracer emerging as an alternative to the routinely used ^{68}Ga-PSMA-11 for evaluating the extent of disease in PCa patients. Recent retrospective studies by Giesel et al. (*18*) and Rahbar et al. (*19*) have shown high detection rates with ^{18}F-PSMA-1007 in biochemical failure—rates comparable or superior to those reported for ^{68}Ga-PSMA-11, even in patients with low PSA levels (≤0.5 ng/mL). This finding may have a significant impact on the further management of the disease.

The present study was a prospective head-to-head comparison of the performance of ^{68}Ga-PSMA-11 and ^{18}F-PSMA-1007 in staging intermediate- and high-risk PCa in the same patients using histopathologic and immunohistochemical analysis as the reference standard. The results of this study show good concordance between the radiotracers; both performed equally well and showed high accuracy in detection of the dominant intraprostatic lesion. In view of the near-equal performance of the 2 tracers, this preliminary study suggests the routine use of ^{18}F-PSMA-1007 in lieu of ^{68}Ga-PSMA-11 for staging PCa patients, and clinicians can use either radiotracer based on availability. The present study also provides further validation as to the role of labeled PSMA in the staging of newly diagnosed PCa patients, an indication that has not been studied as extensively as in the biochemical-failure setting.

On the basis of visual analysis, ^{18}F-PSMA-1007 may identify additional low-intensity small intraprostatic lesions, which can result in an increased false-negative rate or detection of clinically irrelevant low-grade tumors. The clinical relevance, if any, of the latter may be limited in the context of treatment of patients with higher-grade dominant lesions.

In view of the almost negligible urinary excretion, ^{18}F-PSMA-1007 may enable a more accurate interpretation of tumor lesions located near physiologic urine uptake. However, this possible advantage was not clearly demonstrated in the present study and should be further explored.

None of the patients included in this study had lymph node involvement, despite the fact that more than half the patients in this small cohort had either high-risk or unfavorable intermediate-risk PCa. Thus, a comparison of the ability of the 2 tracers to detect lymph node involvement could not be done.

Some limitations need to be highlighted. First, this was a small pilot study that needs to be corroborated in a larger cohort. Second, long-term follow-up is still unavailable. Third, 2 patients had false-positive small foci of intraprostatic uptake, irrespective of the dominant lesion, that were actually sites of chronic inflammation. These areas showed weak PSMA staining on immunohistochemistry. Rahbar et al. (*33*) also showed evidence of false-positive uptake in areas of prostatitis. This should be kept in mind as a potential drawback when interpreting less intense foci of intraprostatic uptake. Administration of furosemide concomitant with ^{68}Ga-PSMA-11, as recommended by some authors (*34*), was not implemented until recently in our local protocol. This is a major drawback to this study, as uptake of ^{68}Ga-PSMA-11 in the urinary tract would have been lower and might resemble that of ^{18}F-PSMA-1007.

Another major limitation of this study is the different uptake time used for the 2 radiotracers. For ^{68}Ga-PSMA-11, the acquisition was performed between 45 and 80 min after injection, whereas ^{18}F-PSMA-1007 PET/CT was performed 60 min after injection. These uptake periods were derived from the literature (*24,34,35*). Theoretically, a longer uptake may lead to an improved tumor-to-background ratio (*34,35*) and result in bias in favor of the tracer for which a longer uptake was applied. However, in a busy routine clinical practice, we failed to perfectly match the uptake time for the 2 tracers.

CONCLUSION

This pilot study shows that both ^{18}F-PSMA-1007 and ^{68}Ga-PSMA-11 identify all dominant prostatic lesions in patients with intermediate- and high-risk PCa at staging. ^{18}F-PSMA-1007, however, may detect additional low-grade lesions of limited clinical relevance.

DISCLOSURE

No potential conflict of interest relevant to this article was reported.

ACKNOWLEDGMENTS

We thank our dedicated technicians for their contribution to this work.

KEY POINTS

QUESTION: How does ^{18}F-PSMA-1007 PET/CT perform in comparison to ^{68}Ga-PSMA-11 PET/CT in staging PCa?

PERTINENT FINDINGS: A prospective intraindividual comparison was made between ^{68}Ga-PSMA-11 and ^{18}F-PSMA-1007 for staging PCa in 16 patients scheduled to undergo radical prostatectomy. Histopathologic specimens were used as a reference standard. The results of this study show both radiotracers to have comparably high detectability for the dominant intraprostatic lesion.

IMPLICATIONS FOR PATIENT CARE: The results of this study suggest the routine use of either ^{18}F-PSMA-1007 or ^{68}Ga-PSMA-11 for staging PCa.

REFERENCES

1. Afshar-Oromieh A, Malcher A, Eder M, et al. PET imaging with a [^{68}Ga]gallium-labelled PSMA ligand for the diagnosis of prostate cancer: biodistribution in humans and first evaluation of tumour lesions. *Eur J Nucl Med Mol Imaging.* 2013;40:486–495.
2. Maurer T, Gschwend JE, Rauscher I, et al. Diagnostic efficacy of ^{68}gallium-PSMA positron emission tomography compared to conventional imaging for lymph node staging of 130 consecutive patients with intermediate to high risk prostate cancer. *J Urol.* 2016;195:1436–1443.
3. Afshar-Oromieh A, Avtzi E, Giesel FL, et al. The diagnostic value of PET/CT imaging with the ^{68}Ga-labelled PSMA ligand HBED-CC in the diagnosis of recurrent prostate cancer. *Eur J Nucl Med Mol Imaging.* 2015;42:197–209.
4. van Leeuwen PJ, Emmett L, Ho B, et al. Prospective evaluation of ^{68}gallium-prostate-specific membrane antigen positron emission tomography/computed tomography for preoperative lymph node staging in prostate cancer. *BJU Int.* 2017;119:209–215.
5. Herlemann A, Wenter V, Kretschmer A, et al. ^{68}Ga-PSMA positron emission tomography/computed tomography provides accurate staging of lymph node regions prior to lymph node dissection in patients with prostate cancer. *Eur Urol.* 2016;70:553–557.
6. Öbek C, Doğanca T, Demirci E, et al. The accuracy of ^{68}Ga-PSMA PET/CT in primary lymph node staging in high-risk prostate cancer. *Eur J Nucl Med Mol Imaging.* 2017;44:1806–1812.
7. Afshar-Oromieh A, Zechmann CM, Malcher A, et al. Comparison of PET imaging with a ^{68}Ga-labelled PSMA ligand and ^{18}F-choline-based PET/CT for the diagnosis of recurrent prostate cancer. *Eur J Nucl Med Mol Imaging.* 2014;41:11–20.
8. Eiber M, Maurer T, Souvatzoglou M, et al. Evaluation of hybrid ^{68}Ga-PSMA ligand PET/CT in 248 patients with biochemical recurrence after radical prostatectomy. *J Nucl Med.* 2015;56:668–674.
9. Morigi JJ, Stricker PD, van Leeuwen PJ, et al. Prospective comparison of ^{18}F-fluoromethylcholine versus ^{68}Ga-PSMA PET/CT in prostate cancer patients who have rising PSA after curative treatment and are being considered for targeted therapy. *J Nucl Med.* 2015;56:1185–1190.
10. Uprimny C. ^{68}Ga-PSMA-11 PET/CT: the rising star of nuclear medicine in prostate cancer imaging? *Wien Med Wochenschr.* 2019;169:3–11.
11. Rauscher I, Maurer T, Beer AJ, et al. Value of ^{68}Ga-PSMA HBED-CC PET for the assessment of lymph node metastases in prostate cancer patients with biochemical recurrence: comparison with histopathology after salvage lymphadenectomy. *J Nucl Med.* 2016;57:1713–1719.
12. Fendler WP, Calais J, Eiber M, et al. Assessment of ^{68}Ga-PSMA-11 PET accuracy in localizing recurrent prostate cancer: a prospective single-arm clinical trial. *JAMA Oncol.* 2019;5:856–863.
13. Fendler WP, Schmidt DF, Wenter V, et al. ^{68}Ga-PSMA PET/CT detects the location and extent of primary prostate cancer. *J Nucl Med.* 2016;57:1720–1725.
14. Kesch C, Kratochwil C, Mier W, Kopka K, Giesel FL. ^{68}Ga or ^{18}F for prostate cancer imaging? *J Nucl Med.* 2017;58:687–688.
15. Giesel FL, Hadaschik B, Cardinale J, et al. F-18 labelled PSMA-1007: biodistribution, radiation dosimetry and histopathological validation of tumor lesions in prostate cancer patients. *Eur J Nucl Med Mol Imaging.* 2017;44:678–688.
16. Rahbar K, Weckesser M, Ahmadzadehfar H, Schäfers M, Stegger L, Bögemann M. Advantage of ^{18}F-PSMA-1007 over ^{68}Ga-PSMA-11 PET imaging for differentiation of local recurrence vs. urinary tracer excretion. *Eur J Nucl Med Mol Imaging.* 2018;45:1076–1077.
17. Giesel FL, Cardinale J, Schäfer M, et al. ^{18}F-labelled PSMA-1007 shows similarity in structure, biodistribution and tumour uptake to the theragnostic compound PSMA-617. *Eur J Nucl Med Mol Imaging.* 2016;43:1929–1930.
18. Giesel FL, Knorr K, Spohn F, et al. Detection efficacy of [^{18}F]PSMA-1007 PET/CT in 251 patients with biochemical recurrence after radical prostatectomy. *J Nucl Med.* 2019;60:362–368.
19. Rahbar K, Afshar-Oromieh A, Seifert R, et al. Diagnostic performance of ^{18}F-PSMA-1007 PET/CT in patients with biochemical recurrent prostate cancer. *Eur J Nucl Med Mol Imaging.* 2018;45:2055–2061.
20. Mottet N, Bellmunt J, Bolla M, et al. EAU-ESTRO-SIOG guidelines on prostate cancer. Part 1: screening, diagnosis, and local treatment with curative intent. *Eur Urol.* 2017;71:618–629.
21. Amor-Coarasa A, Kelly JM, Gruca M, Nikolopoulou A, Vallabhajosula S, Babich JW. Continuation of comprehensive quality control of the itG ^{68}Ge/^{68}Ga generator and production of ^{68}Ga-DOTATOC and ^{68}Ga-PSMA-HBED-CC for clinical research studies. *Nucl Med Biol.* 2017;53:37–39.
22. Shamni O, Nebeling B, Grievink H, Mishani E. Fine-tuning of the automated [^{18}F] PSMA-1007 radiosynthesis. *J Labelled Comp Radiopharm.* 2019;62:252–258.
23. Cardinale J, Martin R, Remde Y, et al. Procedures for the GMP-compliant production and quality control of ^{18}F-PSMA-1007: a next generation radiofluorinated tracer for the detection of prostate cancer. *Pharmaceuticals (Basel).* 2017;10:1–18.
24. Rauscher I, Krönke M, König M, et al. Matched-pair comparison of ^{68}Ga-PSMA-11 and ^{18}F-PSMA-1007 PET/CT: frequency of pitfalls and detection efficacy in biochemical recurrence after radical prostatectomy. *J Nucl Med.* June 28, 2019 [Epub ahead of print].
25. Uprimny C, Kroiss AS, Decristoforo C, et al. ^{68}Ga-PSMA-11 PET/CT in primary staging of prostate cancer: PSA and Gleason score predict the intensity of tracer accumulation in the primary tumour. *Eur J Nucl Med Mol Imaging.* 2017;44:941–949.
26. Rauscher I, Maurer T, Fendler WP, Sommer WH, Schwaiger M, Eiber M. ^{68}Ga-PSMA ligand PET/CT in patients with prostate cancer: how we review and report. *Cancer Imaging.* 2016;16:14.
27. Ceci F, Uprimny C, Nilica B, et al. ^{68}Ga-PSMA PET/CT for restaging recurrent prostate cancer: which factors are associated with PET/CT detection rate? *Eur J Nucl Med Mol Imaging.* 2015;42:1284–1294.
28. Hofman MS, Hicks RJ, Maurer T, Eiber M. Prostate-specific membrane antigen PET: clinical utility in prostate cancer, normal patterns, pearls, and pitfalls. *Radiographics.* 2018;38:200–217.
29. Landis JR, Koch GG. The measurement of observer agreement for categorical data. *Biometrics.* 1977;33:159–174.
30. Zelefsky MJ, Pei X, Chou JF, et al. Dose escalation for prostate cancer radiotherapy: predictors of long-term biochemical tumor control and distant metastases-free survival outcomes. *Eur Urol.* 2011;60:1133–1139.
31. Zumsteg ZS, Zelefsky MJ. Short-term androgen deprivation therapy for patients with intermediate-risk prostate cancer undergoing dose-escalated radiotherapy: the standard of care? *Lancet Oncol.* 2012;13:e259–e269.
32. Calais J, Fendler WP, Herrmann K, et al. Comparison of ^{68}Ga-PSMA-11 and ^{18}F-fluciclovine PET/CT in a case series of 10 patients with prostate cancer recurrence. *J Nucl Med.* 2018;59:789–794.
33. Rahbar K, Weckesser M, Huss S, et al. Correlation of intraprostatic tumor extent with ^{68}Ga-PSMA distribution in patients with prostate cancer. *J Nucl Med.* 2016; 57:563–567.
34. Fendler WP, Eiber M, Beheshti M, et al. ^{68}Ga-PSMA PET/CT: joint EANM and SNMMI procedure guideline for prostate cancer imaging: version 1.0. *Eur J Nucl Med Mol Imaging.* 2017;44:1014–1024.
35. Rahbar K, Afshar-Oromieh A, Bögemann M, et al. ^{18}F-PSMA-1007 PET/CT at 60 and 120 minutes in patients with prostate cancer: biodistribution, tumour detection and activity kinetics. *Eur J Nucl Med Mol Imaging.* 2018;45:1329–1334.